

# MEASURING SPECKLE CORRELATION USING AN FPGA SYSTEM

By

TIMOTHY HOLMES

A masters thesis submitted in the partial fulfillment of  
the requirements for the degree of

MASTER OF SCIENCE

DEPAUL UNIVERSITY  
Department of Physics and Astrophysics

NOVEMBER 2021

© Copyright by TIMOTHY HOLMES, 2021  
All Rights Reserved



To the Faculty of DePaul University:

The members of the Committee appointed to examine the thesis of TIMOTHY HOLMES find it satisfactory and recommend that it be accepted.

---

Eric Landahl, Ph.D., Chair

---

Eric Landahl, Ph.D.

---

Committee Member C, Ph.D.

## ACKNOWLEDGMENT

# MEASURING SPECKLE CORRELATION USING AN FPGA SYSTEM

Abstract

by Timothy Holmes,  
DePaul University  
November 2021

Research Advisor: Eric Landahl

Put Abstract here

# TABLE OF CONTENTS

# LIST OF TABLES

# LIST OF FIGURES



## **Dedication**

This thesis is dedicated to my father for supporting and encouraging my interest in science from the beginning. I would not have come this far without his hard work and love.

I am indebted to the staff and scientists at Fermilab and Matthew Wetstein for boosting my scientific curiosity. Eric Landahl for making the pattern recognition measurements possible, and for providing me with an unparalleled scientific environment to grow in. Finally, Ellek Linton for sharing Machine Learning expertise and a pint off the coast in California.

# Chapter One

## INTRODUCTION

### 1.1 Thesis Overview

This thesis proposes a new analysis method for extracting information from the complex, fluctuating visible light patterns that are formed when coherent light is scattered from small particles suspended in solution.

The first chapter of this thesis begins with a review of the microscopic random motion of a small particle in an idealised solution, specifically a “Newtonian fluid”. The motion is described as a random walk termed “Brownian motion”, and is consistent with the macroscopic theory of diffusion. Next, I consider the scattering of light by a single such particle, and then identify certain assumptions that can be made to extend these results to a collection of randomly moving particles. These results suggest several different methods that can be used to determine the particle size from light scattering. The techniques can be broadly classified into two groups: those that measure spatial correlations in scattered light intensity, and those that measure temporal correlations. Several of these approaches are in routine use in analytical laboratory equipment today. The introductory chapter ends with a simple “kitchen table” experimental demonstration of the Dynamic Light Scattering phenomenon, which produces what appears to be a randomly fluctuating “speckled” pattern – but in fact

contains spatial and temporal correlations which depend on the composition of the scattering material.

In the second chapter, I present the difficulties inherent in analysing these Speckle patterns using existing methods. These limitations are found to mostly result from the assumptions that were required for analytical solutions presented in the previous chapter. For several important applications, these limitations can be severe. I then review a recent development (**LeeS**), termed “double-pulse speckle”, that demonstrated simultaneous recording of spatial and temporal light correlations and presented an analysis technique for extracting particle size using computational spatial convolutions of the experimentally temporally correlated light scattering data. Importantly, this technique has been implemented in a relatively inexpensive and compact optical apparatus by my DePaul Physics Department colleague, Kyle Napoleon, who provided the dataset used in this thesis. The data set consists of visible laser-light scattering images recorded at multiple time-correlation delays, taken on standard calibration samples consisting of manufactured latex spheres (90 nm, 300 nm, and 490 nm diameters) in water at controlled dilutions and mixtures.

The use of computational spatial convolutions to extract particle size from double-pulse speckle images provides the motivation for this thesis. The results of **LeeS** do not provide an unambiguous answer about the grid spacing or weighting that should be used in the spatial convolutions, nor do they provide any guidance for extracting particle sizes from mixtures of different particles, for averaging out noise from non-ideal signal levels, or from extracting composition when modelling the scattering from first principles is difficult. A model-independent method for empirical particle identification is desirable. In the third Chapter, I review the underlying principles of Convolutional Neural Networks (CNN), an emerging machine learning approach to image classification that relies on optimising repeated spatial convolutions.

The fourth chapter of this thesis describes what is to the best of my knowledge the first attempt to train a CNN to recognise light scattering images produced using the double-pulse speckle experimental approach. The data set as provided had to be processed, labelled, and then reduced in size to be computationally tractable. Initial attempts at training a few-layer CNN were successful, demonstrating the model-independent ability to sort samples by composition from the double-pulse speckle images.

In conclusion, I wrap up this thesis in the final chapter summarising the context of this thesis at large. Including some implications, drawbacks and advantages of using CNN in double-pulse DLS.

## 1.2 Newtonian Fluids

By definition, a liquid does not support shear stress in equilibrium. Any forces applied to a liquid will cause it to flow and thereby relieve the stress. Before equilibrium is reached, however, a moving liquid can support a shear stress that is due to internal, velocity-dependent friction. A simple one-dimensional example is described in the Feynman Lectures (**Feynman**), shown in Fig. 1.1. The example consists of two parallel plates of area  $A$  separated by a distance  $d$  that is filled by a fluid, and when one plate is dragged by an external force  $F$ , it moves at a constant velocity  $v_0$ , described by  $F/A = \eta v_0/d$ , where  $\eta$  is a proportionality constant named the coefficient of viscosity. A liquid that is both incompressible and obeys this linear dependence of shear stress  $F/A$  on velocity is called a “Newtonian fluid”. From this equation, the SI units of viscosity are  $\text{kg}/(\text{m} \cdot \text{s})$ . This thesis uses water at room temperature as the solution in which particles are suspended, with a viscosity near  $10^{-3} \text{kg}/(\text{m} \cdot \text{s})$ , (**Feynman**).

Motion in Newtonian fluids can be characterised by a dimensionless parameter called  $Re$ , or the Reynold's number.  $Re$  is the ratio of the inertial forces to the drag forces in a fluid, or

$$Re = \frac{F_{inertial}}{F_{drag}}. \quad (1.1)$$

Following (**Purcell**), consider an object with a characteristic length dimension  $a$  moving in a Newtonian fluid, as shown in Fig. 1.1. The inertial forces are found from Newton's Second Law,

$$F_{inertial} = \frac{dp}{dt} = v \frac{dm}{dt}. \quad (1.2)$$

where  $p$  is the momentum of the displaced fluid,  $v$  is its velocity,  $m$  is its mass, and derivatives are taken with respect to time  $t$ . The mass flow rate  $dm/dt$  can be found by multiplying the density  $\rho$  by the volume flow rate  $dV/dt$ ,

$$\frac{dm}{dt} = \rho \frac{dV}{dt} = \rho v A \quad (1.3)$$

where  $v$  is the velocity of the object with an area  $A$ . Combining Eqs. 1.1 and 1.2, the inertial force of the moving object can be written as

$$F_{inertial} = \rho A v^2 \quad (1.4)$$

The drag force can be estimated by rearranging Eq. 1.4,

$$F_{drag} = A \nu \eta / a \quad (1.5)$$

where I have assumed that the size of the plate in Fig. 1.1 plays a similar role to the size

of the object in Fig. 1.2 when determining the drag force, and that the velocity is constant. The Reynolds number is therefore given by

$$Re = \frac{F_{inertial}}{F_{drag}} = a\rho\nu/\eta \quad (1.6)$$

When  $Re < 1$ , viscous drag is more important than inertia in determining particle motion in a fluid, i.e. the particle will slow down in a relatively short space and brief time. This is more likely to be the case for smaller particle sizes moving at slower speeds in highly viscous fluids.

*“If you are very low Reynolds number, what you are doing at the moment is entirely determined by the forces that are exerted on you at that moment, and by nothing in the past.”*  
(**Purcell**)

The relative lack of inertial memory, contrary to the usual interpretation of Newton’s First Law, results in a random walk, discussed in the next section.

For the special case of a spherical particle in a Newtonian fluid, the drag force in Eq. 1.5 can be exactly calculated as

$$F_{drag} = 6\pi a\eta\nu \quad (1.7)$$

a result known as Stoke’s Law (**Feynman**).

## 1.3 Brownian motion

A fluid is ultimately made of molecules (such as water molecules) which are undergoing thermal motion at room temperature. These molecules will bombard our particle from all sides

irregularly, causing small collisions that can impart momentum changes. These collisions happen often, perhaps  $10^{14}$  times per second (**Reif**). Although these collisions are random, they will add up to an increasing distance moved away from an initial position over time. Observations of the microscopic motion of small particles show that they do indeed slowly drift within a fluid. The Newtonian fluid model can be used to estimate this drift speed, or the mean squared distance travelled by a particle in a given amount of time.

Following (**Reif**), the equation of motion in one dimension,  $x$ , for a particle in a Newtonian fluid (with drag proportional to the velocity) undergoing an arbitrary external force can be written as

$$F_{ext} = ma + F_{drag} = m \frac{d^2x}{dt^2} + \mu \frac{dx}{dt} \quad (1.8)$$

where  $\mu$  is a drag coefficient dependent upon the viscosity and particle size, e.g.  $6\pi a\eta$  from Eq. 1.8 above. Multiplying the equation by the position  $x$  and taking the time average yields

$$\left\langle mx \frac{d^2x}{dt^2} \right\rangle + \mu \left\langle x \frac{dx}{dt} \right\rangle = \langle x F_x \rangle \quad (1.9)$$

First consider the term on the right hand side of the equation. For Brownian motion, the  $x$ -component of the external force  $F_x$  comes from a random collision with a water molecule, which can be in any direction relative to  $x$ . For any given location of  $x$ , there is no reason why  $F_x$  should be positive or negative, and motion in either direction is equally likely, so the time average of the product of  $x$  and  $F_x$  is zero. The first term on the left hand of the equation can be re-written as

$$mx \frac{d^2x}{dt^2} = m \frac{d[x(dx/dt)]}{dt} - m \left( \frac{dx}{dt} \right)^2. \quad (1.10)$$

The second term on the right hand side of Eq. 1.10 can be re-written as

$$x \frac{dx}{dt} = \frac{1}{2} \frac{d}{dt} \langle x^2 \rangle. \quad (1.11)$$

Combining Eqs. 1.8 through 1.10 yields

$$-\langle mv^2 \rangle + \frac{\mu}{2} \frac{d}{dt} \langle x^2 \rangle = 0. \quad (1.12)$$

According to kinetic theory, the kinetic energy of the particle should have a mean value of  $1/2kT$ , where  $k$  is Boltzmann's constant and  $T$  is the temperature. Inserting this equivalence the average drift in one dimension can be related to the viscosity and the temperature,

$$\frac{d\langle x^2 \rangle}{dt} = 2 \frac{kT}{\mu} \quad (1.13)$$

This result shows that a particle will move due to Brownian motion at a rate that increases with temperature and decreases with the drag coefficient. In three dimensions, and for the special case of a small sphere in a Newtonian fluid, this is equivalent to a diffusion coefficient  $D$ ,

$$D = \frac{kT}{6\pi a\eta} \quad (1.14)$$

This result is referred to as the Stokes-Einstein relation (**Feynman**). Table 1.1 shows a list of major assumptions required to relate the diffusion coefficient to temperature, viscosity, and particle size.

## 1.4 Dynamic Light Scattering

Quasi-Elastic Light Scattering, better known as Dynamic Light Scattering (DLS) is a technique in soft-matter physics exploited to calculate particles' distribution and size in the



ASSUMPTIONS	ORIGIN OF ASSUMPTIONS
Fluid is incompressible	Newtonian fluid
Fluid has a linear drag coefficient	Newtonian fluid
Particle is small	Low Reynolds number, Brownian motion
Spherical shape particle	Stokes-Einstein relation

**Table 1.1** List of assumptions made in the analysis of small particle motion.

sub-micron region. The technique utilises a temporal autocorrelation function of scattered light over time given by particle diffusing according to Stokes-Einstein relation in Eq. 1.14. The time dependency fluctuations in the diffused light are measured by a fast photon counter on the opposite side of the sample. DLS is based on the Brownian motion of diffused-and-dispersed particles of various sizes, forms and properties. When particles are immersed in fluid, they generally move in a random walk, with a characteristic scattering time between scattering events. Such collisions and recoil provokes a specific amount of energy to be transferred, inducing particle movement. The energy transfer is on average constant; therefore has a magnified effect on smaller particles. As a result, smaller particles move with greater momentum than larger particles. Given all known parameters, with their influence on the particle movement, the hydrodynamic radius can be measured by calculating the speed of the particles (**Reif**).

Rayleigh scattering refers to the elastic scattering of light by particles significantly smaller than the wavelength of the radiation. This thesis analyses light scattering at an optical wavelength of 650 nm from a standard set of latex spheres (obtained from Ted Pella, Inc.) with diameters of 90, 300, and 490 nm which are suspended in water at concentrations of  $10^{-5}$ ,  $10^{-6}$ , and  $10^{-7}$  fractional weight per volume. At these concentrations, the suspension appears optically transparent, and only single light scattering events are likely within a 1

cm long scattering path. Rayleigh scattering would predict that a single spherical particle would produce an azimuthally scattering intensity pattern  $I(\theta)$ .

$$I = I_0 \frac{1 + \cos^2 \theta}{2R^2} \left( \frac{2\pi}{\lambda} \right)^4 \left( \frac{n^2 - 1}{n^2 + 2} \right)^2 a^6 \quad (1.15)$$

where  $I_0$  is the incident light intensity,  $a$  is the particle radius (45, 150, or 245 nm),  $\lambda$  is the incident light wavelength of 650 nm,  $n$  is the index of refraction of the solution (water), and  $R$  is the distance from the particle to the location where the scattered light intensity is measured. Theta is the angle between the incident beam and the scattered light direction. The Rayleigh scattering pattern should be strongest along the direction of the incident light ( $\theta = 0$ ), and the total scattered intensity is much higher for larger particles.

Although there are only single scattering events (meaning each light ray strikes only one or zero particles when it passes through the solution), many individual particles located at different, random locations within the sample volume will contribute to the measured intensity pattern. If the incident light phases are also random across the particles, the scattering amplitudes add incoherently, and  $(I\theta)$  simply increases linearly with concentration. If coherent light (i.e. from a laser) is used to illuminate the sample instead, a complex interference pattern is observed. The random interferences will result in fluctuating bright and dark spots termed “speckle”. As the particles move around inside the solution due to Brownian motion, this pattern changes. In other words, the light scattering becomes “dynamic”. The goal of this thesis is the development of a new analysis technique to extract the particle’s size from these patterns.

First, I will review the traditional analysis methods for this purpose, which is referred to as Dynamic Light Scattering. As described above, micron to nanometer sized particles sus-

pended in a Newtonian fluid undergo random thermal movements, which is modelled by Stokes-Einstein equation. The Brownian motion causes the mean distance between the particles to change; this causes a Doppler shift between the incident light and scattered light frequencies. The inevitable result of phase interference is that the speckle pattern fluctuates in intensity as a function of time evolution. This is because the light scattered off the particles arrive at the detector with the same phase to interfere constructively to form a bright patch or deconstruct and form a dark patch. However, in the dynamical process, the speckle pattern is in constant motion from the moving particles forming new patterns. The intensity fluctuation rate depends directly on the size of the particles. Particles with small hydrodynamic radius diffuse faster producing rapid fluctuations. On the other hand, larger particles diffuse slowly, therefore the intensity changes more slowly. The dynamical information of the particles can be derived from the intensity correlation functions.

$$g^{(2)}(Q, \tau) = \frac{\langle I(t) \rangle I(t + \tau)}{\langle I(t) \rangle^2} \quad (1.15)$$

where  $I(t)$  is the intensity of the scattered light and  $\tau$  is the lag-time, i.e. the amount that a duplicate intensity trace is shifted from the original before the averaging is performed (Leuchs, Glauber, and Schleich, 2015). The brackets  $\langle \rangle$  denote time integration, which can be extended to the entire time-series collected.

In this time domain analysis, the autocorrelation function (ACF) usually decays starting from zero delay time, and faster dynamics due to smaller particles lead to faster decorrelation of scattered intensity trace. It has been shown that the intensity ACF is the Fourier transformation of the power spectrum, and therefore the DLS measurements can be equally well performed in the spectral domain. (LeeS). It is difficult to directly measure the intensity fluctuations from Brownian motion because the Doppler shifts are relatively small.

As an improvise, an autocorrelator is connected to record the spectrum of frequencies contained in the intensity fluctuations. The correlator compares signals by recording time series and measuring similarities. A signal is compared with itself at distinct time stamps. For a random process such as diffusion there is no correlation between intensities of a signal at large time differences. The intensities are not related for larger time differences, but there is a strong correlation if the signal intensities at time,  $t$  is compared with  $t + \Delta t$ . In other words, at small  $\Delta t$  the diffusing particles do not move far, therefore the scattering intensity changes little. These two correlation functions illustrate the time. Traditional DLS employs the correlation function to analyse and obtain the sample's size.

## 1.5 Spatial dependence of light scattering

Although Rayleigh scattering provides a convenient model for qualitatively understanding DLS, the assumption that particles must be much smaller than the wavelength is a major limitation. It is not true of the data set analysed in this thesis, where some of the particle sizes are only slightly smaller than the wavelength. Relaxing this constraint leads to much more complicated scattering patterns that are sensitive to the shape as well as the size of the particle. This arises when the particle size is large enough that the scattered light phase varies across the particle dimensions, resulting in interference from a single particle (rather than simply from particle to particle as discussed in the previous section. In particular, the dependence on  $\theta$  is no longer simply co-sinusoidal as in Eq. 1.14, with the actual angular distribution taking on the appearance of a spatial Fourier Transform of the particle shape. The analysis of these scattering patterns can yield particle size as well, without the need to temporally correlate the fluctuating light intensity. This is known as Static Light Scattering (SLS), and is used in a few commercial analytical laboratory instruments for particle size determination. Because (SLS) is geometrically sensitive, it lacks some of the robustness of

the DLS technique; however it is especially applicable to scattering wavelengths where there are no readily available coherent sources, such as in the x-ray region of the spectrum. As will be discussed in the next chapter, this thesis aims to exploit some of the additional spatial information available in light scattering.

## 1.6 Simple demonstration

A simple demonstration of a spatially and temporally changing light scattering pattern is shown in Fig. 1.3. A handheld green laser pointer was used to illuminate a few mL of water held in a plastic cuvette. An opaque piece of paper held on a threaded rod casts a shadow to block out the central, unscattered light, allowing a speckle pattern to be observed at a distance of several meters. Scattered light appears after the addition of a drop of coffee creamer to the water. The creamer holds a distribution of particles of different size; the speckles are observed to fluctuate faster at higher angles (away from the center beam block) since they correspond to smaller particles with faster diffusion speeds. This thesis aims to use both the spatial distribution of the speckles and their dynamic fluctuations to extract particle size.

## Chapter Two

# EXPERIMENTAL APPROACHES AND BACKGROUND

### 2.1 Chapter Summary

This chapter presents the difficulties inherent in analyzing Speckle patterns and Dynamic Light Scattering for the purposes of determining the contents in a solution. These difficulties include not just the assumptions made for analysis in the previous chapter, but also come from problems in experimental implementation. The choice of temporal (DLS) versus spatial (speckle) experimental methods requires compromise. A new combination measurement method, double-pulse speckle, can circumvent many of these limitations, but suffers from ambiguity in analysis, for which I propose a new approach using Convolutional Neural Networks in Chapter 3.

### 2.2 Laboratory setup for DLS

The goal of DLS analysis is to measure the light intensity at one scattering angle as a function of time,  $I(t)$ , and then apply Eq. 1.15 to determine the second order temporal correlation

function  $g^2(\tau)$ . Application of models to determine particle size from correlation functions will be reviewed in Section 2.4 below. A DLS experiment is composed of three elements: a source of light, a sample of interest, and a high speed light intensity detector. The approach is shown schematically in Fig. 2.1.

From Eq. 1.14, diffusion happens quicker as particles get smaller. Therefore, to measure as wide a possible size distribution, the detector for  $I(t)$  needs to be fast as possible. An idea of these timescales can come from examination of the data in Fig. 2.1. For the 95 nm particles of Silicon dioxide, a time resolution of  $10\mu s$  (100 kHz bandwidth) would be necessary to recapitulate the full correlation curve. For the 6 nm Ovalbumin particles, a time resolution of  $1\mu s$  (1 MHz bandwidth) is necessary. This explains the reason that only single angular positions are usually recorded for DLS: single pixel, or point photodetectors with MHz bandwidth are widely available throughout the optical range; however area detectors such as the Charge Coupled Devices (CCD) in consumer electronics usually operate near 60 Hz, which is not nearly fast enough to catch rapid DLS from micron-scale particle. Therefore, most of the scattered light, and also most of the information available from the scattering process, is not captured by measuring DLS at a single angle. Because the scattering intensity is angularly dependent, this restriction is especially detrimental for characterising multiple-components systems, which would be expected to look like the curves of Fig. 2.2 for different sized components superimposed at any one given angle.

The loss of total scattered light intensity in single-point DLS measurement becomes further problematic when consideration of sample concentration and the signal-to-noise ratio of the detected light is taken into account. As long as the particles were small compared to the wavelength of the laser with  $d = \lambda/10$ , the scattered particles illuminated by vertically polarised laser were isotropic. The Rayleigh approximation suggests  $I \propto 1/\lambda^4$ ; the inverse relationship means that higher scattering intensity is obtained as the wavelength of the laser

LIMITATIONS	ORIGIN OF LIMITATIONS
Single angle measurement	Detector must be faster than particle motion
High concentrations	Reduce systematic errors
Low concentrations	Eliminate multiple scattering
Limited sample heterogeneity	Scattering intensity scaling; single angle detection

**Table 2.1** List of limitations in single point DLS analysis. These are in additions to limitations that come from the assumptions made in Table 1.1.

used decreases (**Reif**). Rayleigh approximation also implies,  $I \propto d^6$ . In other words, a 50 nanometer particle will scatter  $10^6$  more light than a 5 nanometer particle. The  $d^6$  factor indicates that it is harder to measure a mixture of 1000 nm and 10 nm particles because the contribution to the total light scattered by the small particles will be extremely small. DLS is highly sensitive measurement where a presence of a larger particle, temperature and viscosity change could contribute to larger systematic errors.

Acquiring data along a single point makes it difficult to control for these systematic errors. One mitigation is to increase the sample concentration to improve scattered light intensity, thereby increasing data acquisition speed while reducing systematic drift and detector background levels. Unfortunately, not all samples of interest are available at high concentration (e.g. expensive reagents such as antibodies), and furthermore, the assumptions of the light scattering models, e.g. Eq. 1.15, require only single scattering events for their validity to hold. A summary of the limitations of DLS, which must be taken in conjunction with the general limitations from Table 1.1, are given in Table 2.1.



## 2.3 Speckle measurement

Given the limitations listed in Table 2.1, there is strong motivation for the development of an apparatus to record the entire scattering pattern so that all of the individual speckles can be observed. This requires increasing the frame rate, or the number of images per second that can be recorded by a camera significantly, from tens of Hz to tens of millions of Hz. Although this is an area of active development, particularly for expensive x-ray detectors (**Escauriza**), it is unlikely to result in an inexpensive, field-deployable device soon.

## 2.4 Double pulse speckle

The light scattering experiment composed of three elements: a source of light, a sample of interest, and a high-speed point detector. The light source of choice was a monochromatic, coherent light diode at the left end of the apparatus. CCD was stationed on the far end of the experiment, right after a beam stop, as shown on Figure 2.3. The optical series system consisted of three lenses as shown in Figure 2.3, L1 focuses a laser beam through a spatial filter to increase the beam quality. L2 collimates the filtered laser before the sample. L3 collects the scattered light onto the CCD imaging detector that displays radially concentric diffraction patterns.

Every frame recorded in the double-pulse method contains a speckle contrast pattern at one particular delay,  $\tau$ , and all angles,  $Q$ , given as  $Q = 4\pi \sin \theta / \lambda$ . The frame rate of the camera no longer limits the temporal resolution, or puts a limit on the smallest particles that can be resolved. Instead the frame rate determines the data acquisition rate. A higher frame rate allows data to be collected quicker. Each individual frame must be analyzed to

LIMITATIONS	ORIGIN OF LIMITATIONS
Large number of detector pixels	Cover many angular regions
Small pixel size	Resolve speckle
Uncertainty in correlation mesh	Complex angle dependence of speckle size
Large data sets	Necessary to reduce noise from single frames

**Table 2.2** List of limitations in double-pulse speckle. These are in addition to limitations that come from the assumptions made in Table 2.2, and replace those limitations given for DLS in Table 2.1. Not included are various experimental difficulties (optical alignment, producing brief laser pulses at specific timing, synchronization of the laser and detector, etc.)

determine the angle-dependent contrast separately; averaging frames would simply wash out all contrast. If the area detector’s pixel noise is comparable to the speckle contrast, it will also be difficult to determine the contribution to the correlation from noise (presumably a Gaussian distribution) vs the exponentially-shaped speckle fluctuations.

The double-pulse experiment potentially creates a large data set. Each double-pulse image is an independent, and completely different measurement of the same situation. The most valuable data would be patterns recorded with the highest contrast, corresponding to the briefest delay between the double-pulses. The size of the data set is further increased by the desire to cover a large angular range, while retaining enough pixel resolution to spatially resolve speckles across this entire field of view. In general, different sized particles may have different speckle sizes at different angles, with delay times that vary across the image as well. These uncertainties make it difficult to determine the proper pixel size to perform a mesh, since it may be non-uniform, and depend upon the sample contents, their heterogeneity, and concentration. A summary of limitations of the double-pulse speckle technique is given in Table 2.3, supplanting the DLS limitations in Table 2.2.

## 2.5 Datasets recorded

As long as the particles were small compared to the wavelength of the laser with  $d = \lambda/10$ , the scattered particles illuminated by vertically polarised laser were isotropic. The Rayleigh approximation suggests  $I \propto 1/\lambda^4$ ; the inverse relationship means that higher scattering intensity is obtained as the wavelength of the laser used decreases (**Reif**). Rayleigh approximation also implies,  $I \propto d^6$ . In other words, a 50 nanometer particle will scatter  $10^6$  more light than a 5 nanometer particle. The  $d^6$  factor indicates that it is harder to measure a mixture of 1000 nm and 10 nm particles because the contribution to the total light scattered by the small particles will be extremely small. It implies that light scattered from larger particles will swamp the scattered light from the smaller ones. These approximations were respected in the experiment and injection of the sample in Newtonian fluid were picked with care. Table 2.3 indicates the size, concentration and sample types. The distance between the light source and the sample cuvette is unmoved throughout the experiment. The distance between the detector and the sample is 0.5 meters.

DLS is highly sensitive measurement where a presence of a larger particle, temperature and viscosity change could contribute to larger systematic errors. Most samples in the study were experimented with several different concentration for two reasons. Firstly, multiple concentrations provide better understanding in the systematic uncertainties. Secondly, effects of concentration reflect on a speckle pattern which affects image quality. Henceforth, a multitude of data types for a given sample at different concentrations can filter poorer quality images prior to data pre-processing. This theory is reflected by Malm et. al. (**Malm**). The samples exhibited in Table 2.1 appear in 90, 300, 490 nanometers given our interest in training and classifying speckles at different sizes. The concentration tables another layer to that classification as some scans have identical sizes but were introduced at different concentrations. The hypothesis was that speckle images would differ enough to treat them as

SAMPLES ID	CONCENTRATION	AVERAGE SIZE IN NM
<i>Scan002</i>	$10^{-3}$	490 nm
<i>Scan003</i>	$10^{-4}$	490 nm
<i>Scan004</i>	$10^{-2}$	490 nm
<i>Scan005</i>	$10^{-3}$	300 nm
<i>Scan006</i>	$10^{-3}$	90 nm
<i>Scan007</i>	distilled water	N/A

**Table 2.3** Spherical latex impurities were used in the sample and their average diameter in nanometers is given in the third column. The concentrations at which latex impurities were introduced is provided in this table.

different set of images to the Deep Learning algorithm.

# Chapter Three

## DEEP LEARNING

### 3.1 Chapter overview

This chapter begins with a review of the underlying principles of Convolutional Neural Networks (CNN), a matured deep learning approach to image classification that relies on optimising repeated spatial convolutions. I then describe the data handling used to prepare double-pulse speckle images for training a particular CNN for image classification.

### 3.2 Motivation

The previous chapter describes the use of computational spatial convolution,  $c^2(Q, \tau)$ , to extract the diffusion parameter  $D$  and therefore the particle size  $a$  from double-pulse speckle image, given a lengthy list of assumptions and limitations that are required for this analysis. In particular, it is unclear what the grid spacing or weighting should be used in the spatial convolutions. Furthermore, it is unclear how to best use the additional information available in double-pulse speckle for extracting particle sizes from mixtures of different particles, for averaging out noise from non-ideal signal levels. Extracting composition when modelling the scattering from first principles is difficult.

On the other hand, the double-pulse speckle technique provides a large amount of images, each representing the same mixture, but completely independent due to the random motion of the particles. This suggests using a model-independent method for sorting the double-pulse speckle patterns, i.e. categorising different mixtures by using a subset of labelled data. Although many model-independent methods exist for categorising data (e.g. (**Eric**)), the ideal approach would use a sorting method that depends on spatial convolutions and is trainable. An emerging approach from Artificial Intelligence research is reviewed in this chapter.

### 3.3 Artificial Neural Network

Artificial Neural Networks (NNs) are biologically inspired networks designed to process inputs, train such input, forming probability weighted associations, and ultimately project an output. The naming of many neural network terminologies stem from animal brains. A neuron is a single element on a network with an associated mathematical function that holds an internal state called activation signal. Individual connection link on a network carries information about input signal. A simple neural network, such as a Perceptron, first introduced in 1958 by Frank Rosenblatt, includes an input layer connected to a second layer via connection link and output layer with an expected probabilistic output (**Frank**). In contrast, deep neural networks with more than one hidden layer are harder to train than shallow or less densely connected neural networks. Colloquially, we can take the phrase "neurons that fire together wire together" for granted because artificial neural nets tend to behave in such fashion. An output of a node is calculated by multiplied inputs by weights and an added bias. Weights are values that control the strength of the connection between two neurons. Bias are additional constants attached to neurons and added to the weighted input before

the activation function is applied. Activation functions that live inside neural network layers modify the data they receive and pass it to the next layer. This allows us to model complex non-linear relationships in-between features. Functions such as sigmoid and ReLU (Rectifier Linear Unit) are household names in Deep Learning community. Activation functions are non-linear, continuously differential and fixed range. A simple neural network is shown in Figure 3.1 consisted of 3 hidden layers and an input and an output layer.

In 1999, the MNIST dataset was open-sourced to the AI community for classification. It contained handwritten digits from 0 through 9 collected from Census Bureau employees and high school students (**MNIST**). It took two weeks to train the data to get any meaningful accuracy at that time. Presently, the computation speed has substantially lowered with far superior accuracy. Below is an MNIST image data broken into  $28 \times 28$  pixels. Individual greyscale values range anywhere between 0 and 1; lighter pixel gradients closer to 1.0, darker pixel values near 0.0. The total input neuron is  $28 \times 28 = 784$ . It is shown below as Figure 3.2.

## 3.4 Convolutional Neural Network

A Convolutional Neural Network or CNN or ConvNet is a specialised form of neural network paramount in processing structured grid-like data such as an image data or time-series data. The nomenclature *convolution* arises from the fact that this genre of neural network undergoes a functional analysis convolution operation: a linear operation on two functions of a real-valued argument. A ConvNet must consist of at least one convolutional layer that differs a CNN from a simple neural network. It enjoys multiple cascaded convolution kernels from left to right ending up flattened and ran through a densely connected neural network. The pioneering work by Yann LeCun et. al. in 1998 led to the fundamental architecture of CNN that we are familiar with today. This includes, the accustomed design of input image stack on

the left, CNN layers in the middle, and output on the right stemming from a fully connected neural network. LeCun's network was christened LeNet5 with features such as using convolution to extract spatial features and sparse connection matrix in between layers. (**leCun**)

Say a weighting function  $w(a)$  exists that ensures given several measurements taken from an experiment the recent most (the most relevant) is weighted heavily than earlier ones. The convolution in such measurement looks like (3.1) however the convolution operation would be denoted with the asterisk as in equation (3.2).

$$s(t) = \int x(a)w(t-a)da \quad (3.1)$$

In CNN,  $w$  is a probability density function to ensure the output will be a weighted average i.e. 0 for all negative arguments. Here,  $x$  is referred to as the input of the ConvNet, the function  $w$  is kernel, and the output is the feature map.

$$s(t) = (x * w)(t) \quad (3.2)$$

The need of CNNs arose from the understanding that densely connected neural networks are limited in understanding features within an image. For instance, fully-connected layers of networks treat any two connections from input later equally despite being far apart within the image pixel. This means feature extraction is not prioritised on a normal neural network architecture. The usage of convolutional layers, or patching, in a CNN is analogous to the structure of the visual cortex in human, where a series of layers process an incoming image and identify progressively more complex features. A ConvNet takes in an input image, assign weights and biases to different objects in the image and able to perform classification.

The three important characteristics of the CNN architectures are local receptive fields, shared



weights, and pooling. A *Local receptive field* is a square patch or a little window in input pixels that are linked to a hidden neuron on feature map. Each connection learns a weight as well as the hidden layer learns a bias overall. The benefit of such patching architect is that image information is preserved during this operation rather than directly flattening input pixels. *Shared weights and biases* are maintained in each hidden neuron connected to its local receptive field in order to detect exactly the same feature at different locations in the input image. Convolutional networks are well adapted to the translation invariance of images (**Nielson**). Convolutional architectures are well-adapted to classify images and makes convolutional networks fast to train.

A ConvNet convolves learned features with input data thereby is able to capture the spatial and temporal dependencies using relevant filters. A classic ConvNet architecture consists of the following three layers:

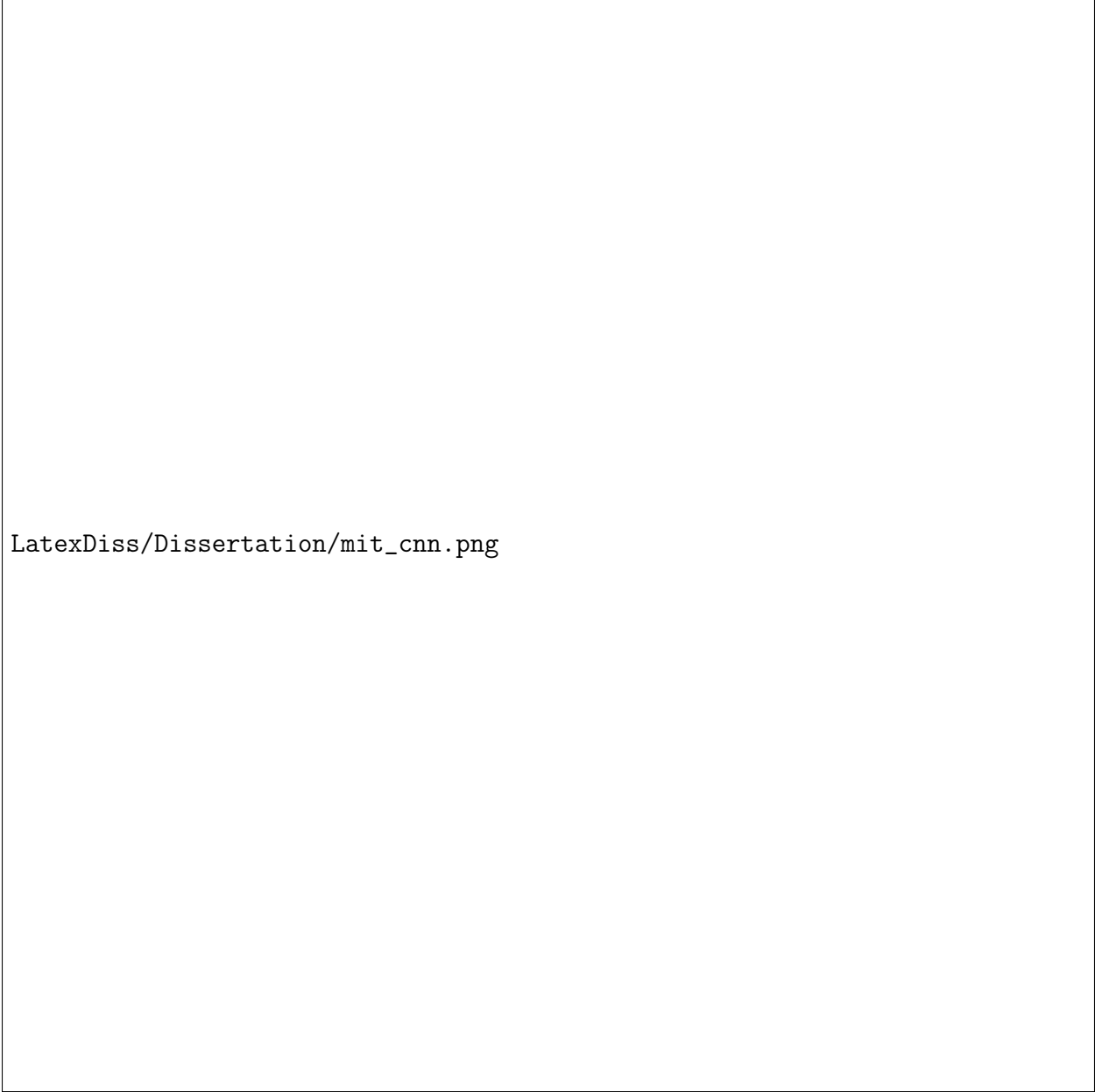
- Convolutional layers + Pooling layers
- Activation layers (ReLU)
- Fully connected Neural Network layers

### 3.4.1 The Convolutional Layer

The convolutional layers are the major foundation in ConvNets; these layers apply a filter to an input causing an activation. A repeated application of filter to an input in activation map is described as the feature map. Feature map indicates metrically the locations and strength of features in an input. The input in the CNN is a tensor which needs to transform into a feature map programmatically. The transformation converts the actual image dimensions into feature map dimension. In computer vision and other image processing applications the convolution is applied routinely. A Gaussian blur  $5 \times 5$  kernel is used to reduce noise, on the left, and a  $3 \times 3$  kernel for detecting edges within the image is shown on the right.

$$\omega = \frac{1}{256} \begin{bmatrix} 1 & 4 & 6 & 4 & 1 \\ 4 & 16 & 24 & 16 & 4 \\ 6 & 24 & 36 & 24 & 6 \\ 4 & 16 & 24 & 16 & 4 \\ 1 & 4 & 6 & 4 & 1 \end{bmatrix} \quad \text{and} \quad \omega = \begin{bmatrix} 0 & -1 & 0 \\ -1 & 4 & -1 \\ 0 & -1 & 0 \end{bmatrix}$$

Mathematically, these operators illustrate how convolutional layers are applied to input. A code block of an application of the convolutional layers is shown below using a Sequential model from the open-sourced Deep Learning library - Keras (discussed more in Analysis section).



LatexDiss/Dissertation/mit\_cnn.png

A Convolutional layer has kernels functions defined by width and height, the number of input and output channels, and the depth of the convolutional filter. The filter is equal to the number channels (depth) of the input feature map.

The pooling layer operates upon each feature map, thus creates a new set of pooled feature maps. The goal of the pooling layer is to reduce the dimensions of the feature maps in

order to lower computation by reducing the learning parameters. The pooling operation involves sliding an appropriate filter of 2 dimension over individual channel of feature map; summarising the features lying within the region covered by the filter. There are three pooling layers: max pooling, average pooling, and global pooling, out of which max pooling is the most popular. Max pooling selects the maximum element of the region of the feature map covered by the filter. After this operation the max-pooling layer becomes a feature map underlying the most prominent feature of the previous feature map. Mathematically, it is done by selecting the largest number from the covered the filter map filter.

### **3.4.2 Activation layer (ReLU)**

The convolution operation is a linear operation but input images are highly non-linear. This non-linearity need is fulfilled by the ReLU operation known to train the network faster than other activation functions. The ReLU or Rectified Linear Unit removes negative values from an activation map by setting them to zero. This method applies the activation function onto the feature map by increasing non-linearity in the network (**Jay**).

### **3.4.3 Fully connected Neural Network layer**

Adding a fully connected layer completes our CNN architecture. It is also a rapid method of learning non-linear combinations of high feature levels. This final layer in the CNN starts with the flattened matrix, which is ultimately connected to every neuron in one layer to every neuron in the other layer. A fully connected layer looks similar to Figure 3.1 once the flattened matrix is connected and ready for classification. The output layer of a fully connected layer uses softmax activation in our study. Softmax is a probability function between 0 and 1, used in multiclass classification. There are multiple speckle images of various samples fed through to make a prediction therefore softmax function was used to make the prediction in the output layer.

## 3.5 Speckle pattern recognition

Images are arrays of structured datatype with some relationship between pixel's edges, lines, and contrasts that are some information that links pixels. A convolution is the simple application of a filter to an input that causes activation. A filter is simply a set of multipliers. Filter could remove vertical or horizontal lines, sharpen or contrast images, and everything in between. Repeated application of the same filter to an input causes a map of activations known as a feature map. The process of image recognition from data to classification goes as follows:

- First, the data collected from the experiment were unzipped into csv (Comma Separated Value) files and uploaded onto a Python script. The imported data contained images into pixels which are numerical values based on their contrast quality. Each Scan has its arrays of images which are in black-and-white form rather than RGB (Red Green Blue) to lower colour channels from 3 to 1 channel.
- The data frame is pre-processed, cleaned by removing unwanted frames, and concatenated. The arrays then go through one-hot encoding which is a process by which categorical variables are converted into integer representation.
- The dataframe is split into training and testing sets at 70:30 percent fraction randomly. This allows to test the model on the training set and measure performance metrics on the test set.
- The dataset, input, is feed through the convolutional layer which performs first feature extraction. Some kernel function, a square matrix, does matrix calculation onto individual pixels. This is passed onto the next layer where maximum value of that pixel is taken. This operation is known as MaxPooling.

- After several convolutional and MaxPooling operations, the dimension of the input is shrunk and ready to be flattened for the fully-connected neural network.
- It starts with the input layer which corresponds to the flattened input from the convolution. Different amounts of hidden layers are assigned based on hyperparameter search that looks for optimised path. Finally an output is allocated with 6 outputs given there were 6 labels in the input for prediction.
- Once the model is trained with at least 20-30 epochs which is a hyperparameter that defines the number times that the learning algorithm will work through the entire training dataset. On the testing set, the model is evaluated on unseen data, thereby model performances are recorded.

Following these steps the classification of sample using supervised CNN was done. These steps can be represented into a figure as shown in Figure (3.3) where the MNIST handwritten digits dataset was the input. Different layers of convolutions and activations were added coupled with a dense neural network architecture. The output layer of the neural network predicted the correct class in the input. In our case, the input has 6 labelled classes and the network was asked to predict the correct class. In Analysis, I discuss these in detail.

The open-sourced libraries used for Deep Learning were Numpy, Pandas and Seaborn for exploratory data analysis, Matplotlib and Pyplot for data visualisation, and Keras and Google's Tensorflow for model architecture. These are publicly available data science libraries, frameworks, and Application Programming Interfaces (APIs) that are widely used for Deep Learning practice.

# Chapter Four

## ANALYSIS

Figure 4.1 was gathered by K. Napoleon and E. Landahl in 2020 at DePaul University where particles of size  $0.49\ \mu m$ ,  $0.3\ \mu m$ ,  $0.09\ \mu m$  were instituted in the DLS experiment. The graph exhibits the DLS in action where the largest diameter particle scattered at the lowest angle shown in blue, conversely the smallest particle, shown in red, scattered at the largest angle. This correlation time against scattering angle was indicative of the Eq. 1.15 in a larger context of seeking relationship off size and correlation time. The Stokes Einstein equation in Eq. 1.14 can be used to obtain the hydrodynamic radius of spheres in non viscous fluid using diffusion equation. Such relationship seeking process is permitted as a consequence of the double-pulse technique. This process provides a spatial correlation(**LeeS**). The implication, therefore, is that spatial information generated by double pulses can determine the size of the particle present in the sample. In data acquisition, Fig 2.1 shows the layout of the apparatus where monochromatic diode laser produces diffraction off the fluid suspended sample and a CCD captures time-stamped images frame by frame. Each scan consists of 500 frames (images) taken with double-pulses of  $100\ \mu s$  duration at the 17 time delays specified below:

$$dt = [10\ 100\ 200\ 300\ 400\ 600\ 800\ 1000\ 1500\ 2000\ 3000\ 4000\ 6000\ 8000\ 10000\ 15000\ 20000]\mu s$$

For instance,  $dt = 10$  implies the camera detector on for  $100\mu s$ , off for  $10\mu s$ , on for  $100\mu s$ . Concentrations are given in dilutions from stock by volume. For instance, a  $10^{-3}$  concentration is 0.1% of the original solution concentration. The solutions are opaque without dilution and the size in nm is the nominal size of the latex spheres in water.

Figures 4.2 - 4.5, the purple colour represents the background in the detector and blue dots represent speckles - higher gradients of blue indicating higher speckles concentration. These figures represent images that are sliced in different dimensions to emphasize different image aspects. Figure 4.2 is one frame of the *Scan005* where  $600 \times 1250$  pixels image shows a ring of constructive and destructive interference pattern. This diffraction pattern generated from the presence of  $300nm$  latex spheres in 0.001 concentration is similar to Fig. 2.4. The major differences are the size and detector sensitivity where Lee et. al. used  $4.5 \mu m$  polystyrene particles, much larger in size than our  $300nm$  spheres. Our CCD detector was an off-the-shelf hardware whilst Lee preferred to use an expensive system of detection. We, nevertheless, obtained similar speckles on our frames. Fig. 4.3 is a  $300 \times 150$  pixels sub-section of the larger scan shown to emphasise on the details of speckles generated on the scan. Figure 4.4 is presented to show the presence of no speckles without any diffraction given no impurity. Figure 4.5 shows *Scan004* with  $1980 \times 1080$  pixels scan which was the maximum possible image the CCD was able to record. All scans produced similar speckles with subtle nuances in the size and locations of speckles harder to detect for a human. However, the CNN was able to learn and recognise those patterns in the images that it was trained on.

The metrics of accuracy and loss are important to judge the performance of the model. Accuracy is the fraction of predictions the model was able to correctly classify. The curse of accuracy metrics is that it varies in the context of use. In other words, the context of the problem defines the accuracy value. For instance, in the case of a brain tumor detection classification, a 96% accuracy of a model might not be ethical to deploy. Whilst if the ac-



SAMPLES	NO. OF PARAMETERS	ACCURACY	LOSS
<i>Scan002 490 nm <math>10^{-3}</math> concentration</i>	49,300,994	0.69	837
<i>Scan003 490 nm <math>10^{-4}</math> concentration</i>	49,218,563	0.89	3569
<i>Scan004 490 nm <math>10^{-2}</math> concentration</i>	49,218,563	0.75	6743
<i>Scan005 300 nm <math>10^{-3}</math> concentration</i>	49,218,563	0.76	3359
<i>Scan006 90 nm <math>10^{-3}</math> concentration</i>	49,218,563	0.78	8317
<i>Scan007 distilled water</i>	N/A	1.00	0.00

**Table 4.1** Types of species used to produce speckle pattern. *Scan007* is a distilled water sample used as a control. The number of parameters is the sum of all weights and biases. Accuracy metric measures the percentage of correct predictions for the test data. Loss function was categorical crossentropy that computes the crossentropy loss between the labels and predictions.

accuracy was evaluated for the case of weather prediction that accuracy might be commercial. In our case, the classification we obtained of about 60% seems appropriate to report in this study as a good one for a prototype. Shown in Figure 4.6, the accuracy versus epochs graph shows how the accuracy is evolving with the number of epochs for collective samples array. Accuracy is To interpret it another way, given the impurities of sizes ranging from 90nm to 490 nm the model should tell you with 60% accuracy what sized sample was present in the cuvette. The For the Loss function that was used off Keras open-sourced library, the imported type was a categorical crossentropy loss. Also known as the softmax loss, and used primarily for multi-class classification, the crossentropy loss trains a CNN to output a probability over the ‘C’ classes for individual image. In a good model, we anticipate the loss to fall as the number of epochs increase. An epoch is a measure of the number of times all of the training vectors are used once to update the weights.

# Chapter Five

## APPLICATIONS

Traditional DLS relies on diffusion coefficient by measuring fluctuations in scattered photon intensity due to particle diffusion. The prevailing application of Dynamic Light Scattering is in analysing particles of size stretching from submicrons to microns such as proteins, nucleic acids, polymers and microorganisms. DLS is simple, highly cost effective, and economical in operate and to transport. DLS is one of the most understood and commercialised techniques in physics to classify particle and profile. A highly accurate, reliable, and replicable analysis is routinely conducted in different laboratories as a result of high accessibility, low cost of the technology. For angular information, a multi-angle DLS is also available off-the-shelf that provides angular independent size results. DLS in the industry is also standardised at International Organisation for Standardisation or ISO standards; such convenience allows easier cross-collaboration between laboratories and even at an international level. This includes but not limited to the size of the sample cuvette, to the light source or scattering angles for various standardised particles.

Our demonstrated novel approach performs concurrent measurements of particles high-speed dynamics producing structural information of the sample. With the aid of of ConvNet image classification, the data analysis portion of speckles is not computationally strenuous, therefore admits to rapid testing. Small in size, economical in nature, the double-pulse ConvNet

DLS is substantiated to be an alternative for non-invasive speckle characterisation. The double-pulse approach advances facilitates DLS to gather richer, high-resolution data at the same or lower cost. The systematic study is easier to conduct in the case of systematic failure running a test. Double-pulse DLS method complemented with a Deep Learning algorithm is a particularly powerful tool. The level of sophistication that a Convolutional Neural Network brings to a traditional DLS is paramount.

DLS hardware setup and Deep Learning software systems are sophisticated yet economical. As a result, the intact set up could be deployed in areas limited in resources. Including, places of natural disaster, low income areas where water quality could be tested cheaply but highly accurately, and rapid fluid analysis for many purposes. A trained DL model backed DLS is applicable in water filtration facilities, marine habitat conservation and monitoring, aquatic agriculture and so on.

# Chapter Six

## SUMMARY

Dynamic light Scattering is a non invasive soft-matter physics technique to scatter light off a sample, thereby obtain spatial information about the sample using temporal data of its intensity. Based on particles fluctuations, a characteristic speckle data is recorded, and ultimately classified to their corresponding hydrodynamic radius. DLS covers a wide range of testing from microscopy to spectroscopy. The technique utilises a temporal auto-correlation function of scattered light over time given by Stokes-Einstein equation. The time dependency fluctuations in the diffused light are measured by a fast photon counter on the opposite side of the sample. DLS is based on the Brownian motion of diffused-and-dispersed particles of various sizes, forms and properties.

Recent new development in double-pulse technique has upstaged traditional DLS. The double-pulse technique leaves the apparatus stage unchanged, rather the novelty appears in swapping the constant stream of laser beam to a well-defined double pulse. This approach measures the transient dynamics from an isolated image rather than dealing with correlation coefficient and lag time. The time-delay between two pulses are such that correlation coefficient measured at the normalised angle covered different decay rates of the speckle. The normalised speckle fringes, captured in time-series images were broken into pixels for Deep Learning image classification. The Convolutional Neural Network extracted features and learned the

differences between classes. Hyperparameters were tuned to optimise the model. Output was a classification performance metrics such as accuracy. In Appendix is shown the loss function that decays as the number of epochs is increased. It shows that as the model is learning off different parameters, it is able to classify correct features within defined labels. The loss function graph is indicative of the model performance.

In spite of drawbacks, DLS enjoys as the top contender for sample identification measurements in submicron regime. The well-established performance of DLS is enhanced by appending it with double-speckle Deep Learning technique as we elaborate in this thesis. Our method can classify macromolecules from an array of species sizes. A major drawback comes at the cost of faster processor or graphic cards to run models faster. A well-trained Convolutional Neural Network classifies the sorts of sample without any painful mathematical modelling of correlation function for individual sample. Rather the model generalises images from trained parameters. An unknown sample classification with accuracy report is possible based on a trained DL model. Overall, our double-pulse technique in conjunction with a Convolutional Neural Network appears superior to classical method of performing DLS. This was a prototype study to measure the feasibility and applicability of Artificial Intelligence in DLS. We are confident that DLS is greatly aided by Deep Learning treatment if not more qualified to classify impurities. More data and higher quality images for training are recommended.

# Chapter Seven

## INTRODUCTION

### 7.1 Thesis Overview

# Chapter Eight

## INTRODUCTION

### 8.1 Thesis Overview

# Chapter Nine

## INTRODUCTION

### 9.1 Thesis Overview



## APPENDIX

# Appendix A

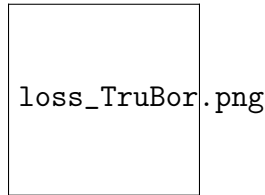


**Figure A.1** Loss against epochs number showing the cost function falling for *Scan002*.